Exp.-Nr. **A2**
Eingang:
an PAC:

# Mainz Microtron MAMI

**A2 Collaboration at MAMI**
Spokespersons: P. Pedroni, A. Thomas

**Proposal for an Experiment**

## "Measurement of photoproduction of $\pi^{\pm}\pi^0$ and $\pi^0\pi^0$ pairs off nuclei"

**Spokespersons for the Experiment :**
Bernd Krusche, Departement für Physik, University of Basel, Switzerland

**Abstract of Physics :**

Photoproduction of mixed-charge pion pairs $\pi^{\pm}\pi^0$ is the key to the understanding of the disappearance of the second and third resonance bump in the total photoabsorption cross section and the related in-medium modifications of the $\rho$ meson and the $D_{13}(1520)$ resonance. Preliminary results from the $\gamma p \to n\pi^+\pi^0$ reaction show that in the second nucleon resonance structure contributions from the $D_{13}(1520) \to N\rho$ decay are of comparable size as contributions from the sequential $D_{13}(1520) \to \Delta\pi$ decay. Data for this reaction from a deuterium target are also under analysis. We will obtain some data for this reaction off $^4$He nuclei together with the already scheduled experiment for the measurement of $\pi\eta$ pairs in view of $\eta$-mesic nuclei and plan to extend this measurements to heavier nuclei. In addition we will measure photoproduction of $\pi^0$ pairs (where no emission of $\rho$-mesons is involved) for comparison.

**Abstract of Equipment :**

The experiment will be performed at the tagged photon facility of MAMI (Glasgow Tagger) using Crystal Ball/TAPS detector setup together with particle identification detector (PID) and multi-wire proportional chambers (MWPCs).

**MAMI Specifications :**

| | |
|---|---|
| beam energy | 1.6 GeV |
| beam polarization | longitudinally polarized |

**Photon Beam Specifications :**

| | |
|---|---|
| tagged energy range | 400 – 1400 MeV |
| photon beam polarization | circularly polarized |

**Equipment Specifications :**

| | |
|---|---|
| detectors | Crystal Ball/TAPS, PID, MWPCs |
| target | liquid $^4$He, solid state targets (Li, C, Ca, Pb) |

**Beam Time Request :**

| | |
|---|---|
| set-up/test with beam | 24 hours |
| data taking | 400 hours |

**List of participating authors:**


- **Institut für Physik, University of Basel, Switzerland**
  S. Abt, S. Garni, M. Günther, A. Käser, B. Krusche, S. Lutterer, Th. Strub, N.K. Walford
- **Institut für Experimentalphysik, University of Bochum, Germany**
  G. Reicherz
- **Helmholtz–Institut für Strahlen- und Kernphysik, University of Bonn, Germany**
  F. Afzal, R. Beck, K. Spieker, A. Thiel
- **JINR, Dubna, Russia**
  N.S. Borisov, A. Lazarev, A. Neganov, Yu.A. Usov
- **SUPA School of Physics, University of Edinburgh, UK**
  M. Bashkanov, S. Kay, D.P. Watts, L. Zana
- **SUPA School of Physics and Astronomy, University of Glasgow, UK**
  J.R.M. Annand, D. Hamilton, D.I. Glazier, S. Gardner, K. Livingston, R.Macrae , I.J.D. MacGregor, C. Mullen, D. Werthmüller
- **Department of Astronomy and Physics, Saint Mary's University Halifax, Canada**
  A.J. Sarty
- **Racah Institute of Physics, Hebrew University of Jerusalem, Israel**
  G. Ron
- **Kent State University, Kent, USA**
  C.S. Akondi, D.M. Manley
- **Institut für Kernphysik, University of Mainz, Germany**
  P. Achenbach, H.J. Arends, M. Biroth, F. Cividini, A. Denig, P. Drexler, M.I. Ferretti-Bondy, W. Gradl, V.L Kashevarov, P.P. Martel, A. Neiser, E. Mornacchi, M. Ostrick, S.N. Prakhov, V. Sokhoyan, C. Sfienti, O. Steffen, M. Thiel, A. Thomas, S. Wagner, J. Wettig, M. Wolfes
- **University of Massachusetts, Amherst, USA**
  R.Miskimen, A. Rajabi
- **Institute for Nuclear Research, Moscow, Russia**
  G. Gurevic, R. Kondratiev, V. Lisin, A. Polonski
- **INFN Sezione di Pavia, Pavia, Italy**
  A. Braghieri, S. Costanza, P. Pedroni
- **Department of Physics, University of Regina, Canada**
  Z. Ahmed, G.M. Huber, D. Paudyal
- **Mount Allison University, Sackville, Canada**
  D. Hornidge
- **Tomsk Polytechnic University, Tomsk, Russia**
  A. Fix
- **George Washington University, Washington, USA**
  W.J. Briscoe, C. Collicott, E.J. Downie, I.I. Strakovski

- **Rudjer Boskovic Institute, Zagreb, Croatia**
  M. Korolija, I. Supek

# 1 Introduction and Motivation

## 1.1 Hadron In-Medium Modifications

The generation of mass via the non-perturbative properties of the strong interaction is a central feature of this force. Unlike any other composite systems, hadrons are objects, which are build out of constituents with masses (2 - 5 MeV for u,d quarks) that are negligible compared to the total mass. Most of the mass is generated by dynamical effects from the interaction of the quarks and an important role is played by the spontaneous breaking of chiral symmetry, the fundamental symmetry of QCD. As a consequence, the lightest baryon, the nucleon, appears at a mass of almost 1 GeV of which only ≈1% are due to the constituent quark masses (see fig.1). The symmetry breaking, which is connected to a non-zero expectation value of scalar $q\bar{q}$ pairs in the vacuum, the chiral condensate, is reflected in the hadron spectrum. Without it, hadrons would appear as mass degenerate parity doublets, which is neither true for baryons nor for mesons. The $J^\pi = 0^-$ pion (the Goldstone boson of chiral symmetry) is much lighter than its chiral partner the $J^\pi = 0^+$ $\sigma$ meson. Similarly, the lowest lying $J^\pi = 1^-$ meson, the $\rho$ has a smaller mass than the $J^\pi = 1^+$ $a_1$ and also the first $J^\pi = 1/2^-$ excited state in the baryon spectrum, the $S_{11}(1535)$, lies much above the $J^\pi = 1/2^+$ nucleon ground state.

However, model calculations (see e.g. Ref. [1]) indicate a temperature and density dependence of the condensate, which is connected to a partial restoration of chiral symmetry at high temperatures and/or large densities. The different regimes are in particular accessible in heavy ion reactions, but the effect is already significant at zero temperature and normal nuclear matter density, i.e. conditions which can be probed with photon and pion beams. One consequence of the partial chiral symmetry restoration is a density dependence of hadron masses. An early prediction for this effect is the so-called Brown-Rho scaling [2]:

$$m^\star_{\sigma,\rho,\omega}/m_{\sigma,\rho,\omega} \approx m^\star_N/m_N \approx f^\star_\pi/f_\pi, \tag{1}$$

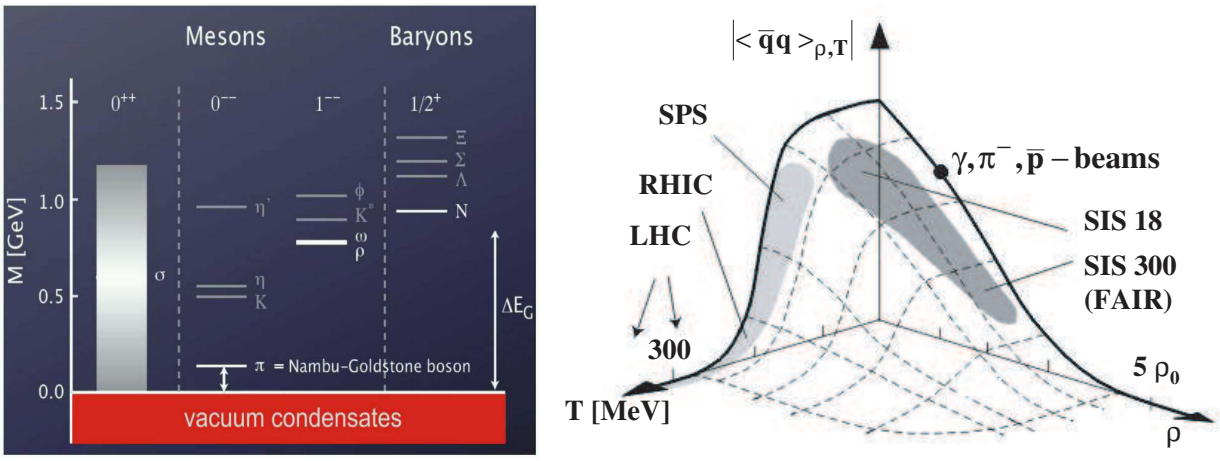


Figure 1: Left hand side: hadrons as excitations of the QCD vacuum. Right hand side: Chiral condensate as function of temperature $T$ and nuclear density $\rho$ ($\rho_o$ normal nuclear matter density)

Although there is no direct relation between the quark condensate and the in-medium properties of hadrons, there is an indirect one via QCD sum rules, which connect the QCD

picture to the hadron picture. In the latter, the in-medium modifications arise from the coupling of mesons to resonance - hole states and the coupling of the modified mesons to resonances. Post, Leupold, and Mosel [3] have calculated the hadron in-medium spectral functions for $\pi$-, $\eta$-, and $\rho$-mesons and baryon resonances in a self-consistent coupled channel approach. The most relevant contributions to the self-energies are shown in the upper part of fig. 2. In the vacuum mesons like the $\rho$ can couple only to meson loops (involving e.g. the pion) and nucleon resonances couple to nucleon - meson loops. However, in the medium mesons can couple to resonance - hole states (the best known example is the coupling of the pion to $\Delta - h$ states in $\Delta$ - hole models). This influences not only the spectral functions of the mesons, but also the resonances which in turn couple to the modified meson loops. It makes necessary an iterative, self-consistent treatment of the self-energies. The predicted effects [3]are in particular large for the $\rho$ meson and the $D_{13}(1520)$ resonance due to the strong coupling of the resonance to $N\rho$. The close by $S_{11}(1535)$ resonance is much less effected in this model (see Fig. 2, bottom). The model results are of course only schematic.

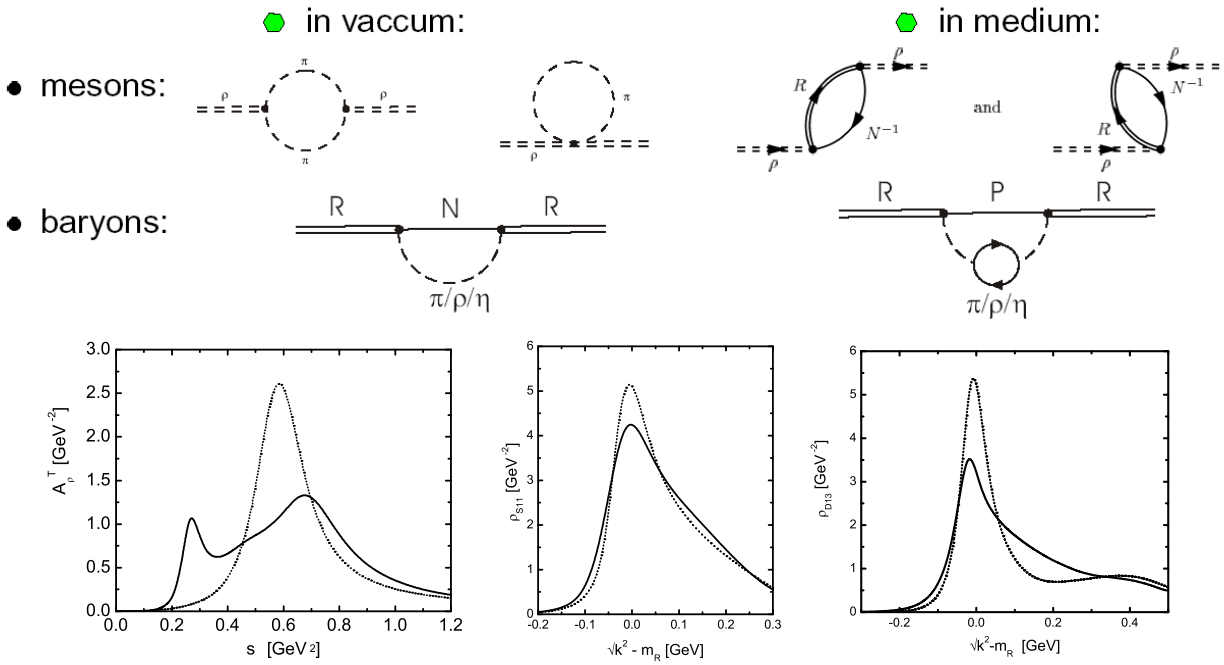


Figure 2: Upper part: diagrams for vacuum and in-medium self-energies of mesons and baryons. [3] Lower part: predicted vacuum (dashed curves) and in-medium (solid curves) spectral functions for the $\rho$ (left), the $S_{11}(1535)$ (center), and the $D_{13}(1520)$ (right) resonances at $q$=0. [3]

Such effects have been searched for in many experiments, using heavy ion and also photon beams (see [4] for a recent review). One example is the study of the $\gamma A \to e^+e^-X$ reaction [5, 6] at the CLAS experiment at Jlab. The $\rho$, $\omega$, and $\phi$ vector mesons could be reconstructed from the invariant mass of the lepton pairs. The disadvantage of using the Dalitz-decay modes of these mesons is of course the small branching ratio into this channel (order of $10^{-5}$ to $10^{-4}$). The advantage of this type of experiment is that, both in the initial and final state, only electromagnetic interaction contribute, so that initial and final state interaction effects are minimized. Due to kinematical limitations only vector

mesons with momenta above 1 GeV could be detected, so that the longer-lived $\omega$ and $\phi$ mesons decayed mostly outside the nuclei without significant in-medium modifications. The short-lived $\rho$ in turn showed a clear broadening of its in-medium width by roughly 70 MeV, but no shift of its mass.

Since the main decay channel of the short-lived $\rho$ meson are pion pairs one should expect a major effect of any in-medium modification of this particle on the production of pion pairs. Furthermore, since the charged $\rho$-mesons $\rho^{\pm}$ decay to $\pi^0\pi^{\pm}$ and the neutral $\rho$ meson to $\pi^+\pi^-$ but (due to isospin conservation) not to $\pi^0\pi^0$ the latter channel can be used for comparison (should be less effected by $\rho$ in-medium effects).

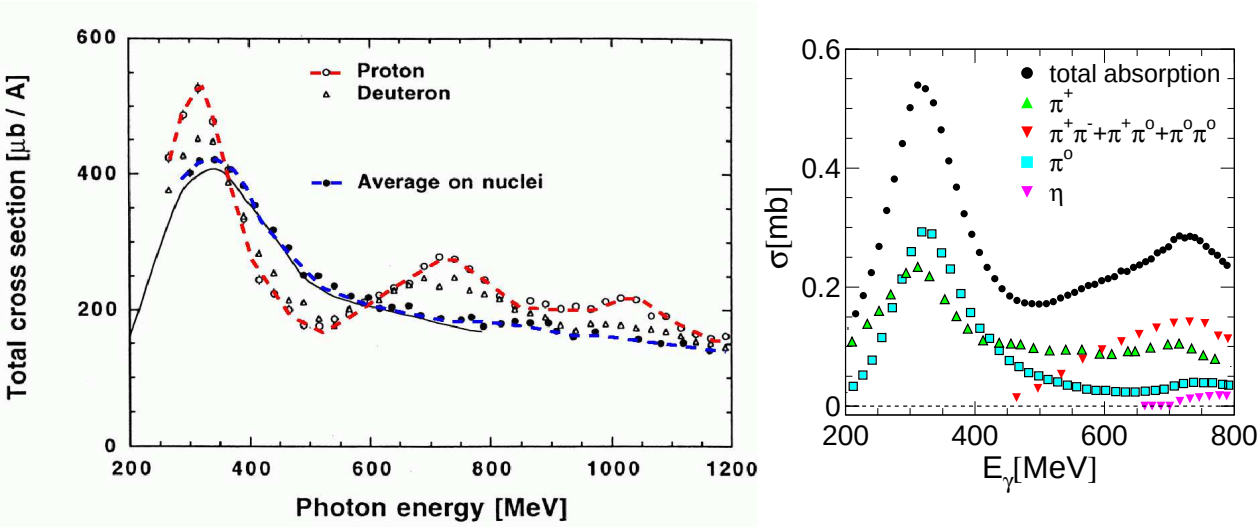


Figure 3: Left hand side: total photoabsorption from the proton, the deuteron and the average for heavy nuclei [7]. Right hand side: Partial cross sections for photoproduction from the proton [8–14].

There is actually a long-known in-medium effect observed in photoproduction reactions off nuclei, which could be related to such effects, but was never really understood: Among the clearest experimental observations of nuclear effects in electromagnetic excitations is the suppression of the second (and third) resonance peaks in total photoabsorption (TPA) on nuclei [7, 15, 16]. The $\Delta$ resonance peak is modified for nuclear targets, but in a way which is consistent with model predictions (see for example [17]). However, TPA on the free proton shows a peak-like structure at incident photon energies between 600 and 800 MeV, which is attributed to the excitation of the $P_{11}(1440)$, $D_{13}(1520)$, and $S_{11}(1535)$ resonances. This structure is not visible for nuclei over a wide range of mass numbers from lithium to uranium. A broadening due to nuclear Fermi motion certainly contributes, but cannot explain the full effect. A simple broadening would at least approximately conserve the integrated cross section, which is obviously not the case. Some authors [18, 19] have argued for an in-medium width of the relevant nucleon resonances, in particular the $D_{13}(1520)$, on the order of 300 MeV. Such an ad hoc assumption brings model predictions close to the data but the justification is not clear. As discussed above Post, Leupold and Mosel [3] find in their coupled channel analysis of the in-medium spectral functions of mesons and resonances a relatively strong broadening of the $D_{13}$ and a much smaller effect for the $S_{11}$. Possible effects resulting from the collisional broadening of the resonances have been studied in detail in the framework of transport models of the BUU-type (see e.g. [20]), but the complete disappearance of the resonance structure was never explained.

The resonance bump on the free proton consists of a superposition of reaction channels with different energy dependencies (see fig. 3, right hand side) which complicates the situation [21]. Much of the rise of the cross section t wards the maximum around 750 MeV is due to the double pion decay channels, in particular to the $n\pi^o\pi^+$ and $p\pi^+\pi^-$ final states. Therefore, it is quite probable that the in-medium behavior of these reactions plays an important role for the observed behavior.

At the time of the observation of the suppression of the second and third resonance bump in total photoabsorption not much was known about the elementary double-pion photoproduction reactions. In particular, the total cross section of the $n\pi^0\pi^+$ final state was significantly underestimated in all models (see [21] for a summary) and almost nothing was known about the production of pion pairs from quasi-free neutrons.

The situation improved after the DAPHNE and TAPS experiments at MAMI studied in detail the pion-pion invariant mass distributions of the $\gamma n \to p\pi^0\pi^-$ [22] and $\gamma p \to n\pi^0\pi^+$ [23] reactions. Both experiments found and excess of strength at large pion-pion invariant masses, which was subsequently interpreted in the framework of the models as a contribution from $D_{13}(1520) \to N\rho$ decays which had previously been neglected in the models due to the fairly large mass of the $\rho$. The results were used in [23] to determine the branching ratio of the $D_{13}(1520)$ state into $N\rho$. These results made it more probable that in-medium effects of the $\rho$ meson could have direct impact on the double-pion production cross sections in the second resonance region because excitation of the $D_{13}(1520)$ resonance is a dominant contribution.

In the meantime, much more information, including also experiments with quasi-free neutrons, has been gathered, which we will shortly summarize in the next section.

## 1.2 Recent Results for Photoproduction of Pion-Pairs off Free and Quasi-Free Nucleons

Photproduction of $\pi^0$ pairs off the free proton has been studied in much detail at the MAMI and ELSA facilities. Precise results for total cross sections, angular distributions, invariant mass distributions of the pion-pion and pion-proton pairs, and beam-helicity asymmetries $I^\odot$, $I^s$, $I^c$ have been published [24–31] and used to extract the contribution of nucleon resonances to this reaction. Results for other polarization observables like target asymmetries $T$, double polarization observables $F$, $H$ are still under analysis. Early attempts to measure the quasi-free $\gamma n \to n\pi^0\pi^0$ reaction have been made in [8, 32, 33]. Recently, detailed results for total cross sections, angular distributions, invariant mass distributions, and beam-helicity asymmetries $I^\odot$ for photoproduction of $\pi^0$ pairs of quasi-free protons and neutrons bound in the deuteron have been published by our group [34,35] and the polarization observables $T$, $F$ for the same reactions are still under analysis.

The most relevant results for the present proposal are summarized in Fig. 4, where the total cross sections for the quasi-free $\gamma p \to p\pi^0\pi^0$ and $\gamma n \to n\pi^0\pi^0$ are shown together with their decomposition into different reaction components. The main contributions in the energy range of the second and third resonance bump stem from sequential resonance decays (intermediate $\Delta\pi^0$ and at higher energies $N^\star\pi^0$ intermediate states) and phase-space contributions which parameterize e.g. the $N^\star \to N\sigma$ decay. The peak of the second resonance region has the same origin for the proton and neutron target. In both cases the sequential $\gamma N \to D_{13}(1520) \to \Delta(1232)\pi^0 \to N\pi^0\pi^0$ decay dominates strongly.

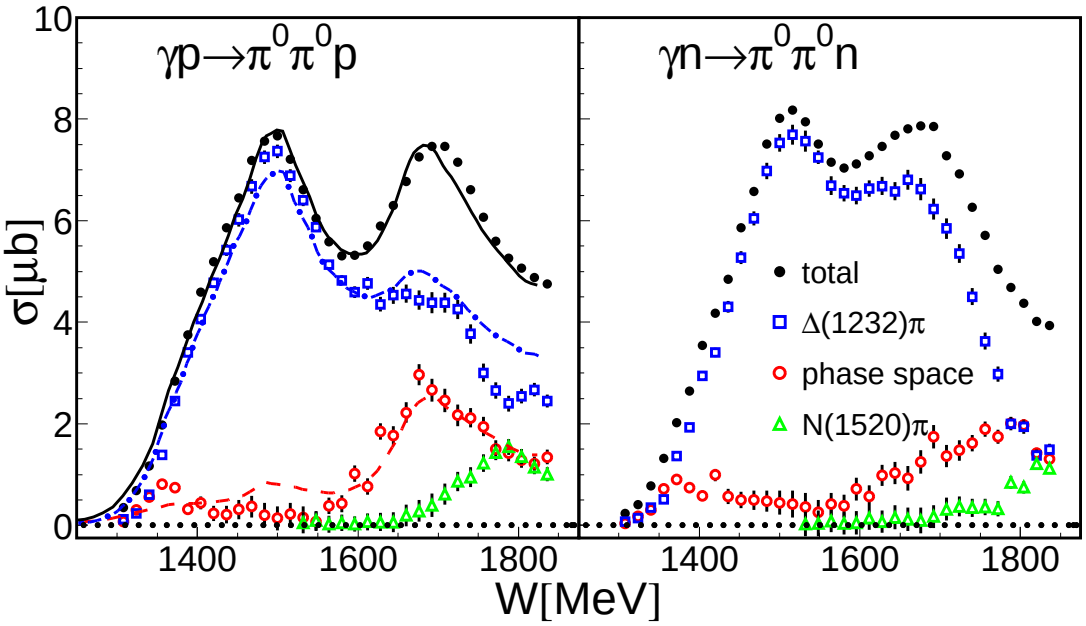


Figure 4: Fitted contributions of the $\gamma N \to \pi^0\Delta(1232)3/2^+ \to \pi^0\pi^0 N$ reaction chain (open blue squares), phase-space decays (open red circles), and $\gamma N \to \pi^0 N(1520)3/2^- \to \pi^0\pi^0 N$ (open green triangles) to the total cross section (filled black circles). Left hand side for the proton target, right hand side for the neutron target. Only for proton target: solid (black), dash-dotted (blue), and dashed (red) curves represent total cross section, sequential decay over $\Delta(1232)3/2^+\pi$ intermediate state, and phase-space component, respectively from a PWA of previous ELSA proton data [24]. All curves renormalized to the total cross section to account for FSI.

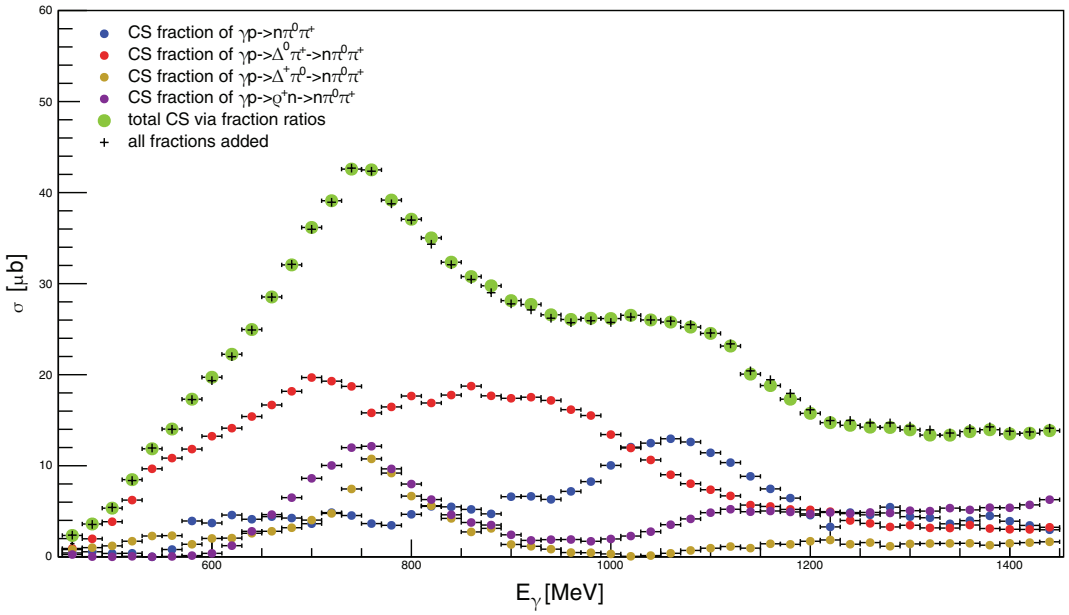


Figure 5: Total cross section for the $\gamma p \to n\pi^+\pi^0$ reaction with partial reaction cross sections for different processes. Green dots and black crosses: total cross section, blue symbols: phase space $\pi^0\pi^+$, red symbols: $\Delta^0\pi^+$ intermediate state, yellow symbols: $\Delta^+\pi^0$ intermediate state, purple symbols: $n\rho^+$ intermediate state.

Double $\pi^0$ production in the second resonance bump is therefore a nice tool to investigate $D_{13}(1520)$ in-medium modifications. The structure of the third resonance bump is more complicated. For the neutron it is still dominated by sequential decays via the $\Delta\pi^0$ intermediate state, but for the proton contributions from phase-space and $N^\star\pi^0$ intermediate states are much more important. The present results provide a good approximation of the average nucleon cross section for heavy nuclei before Fermi smearing and FSI effects.

The data base for the production off $\pi^\pm\pi^0$ pairs of free and quasi-free nucleons is sparse, but the situation will much improve due to data measured at MAMI which is in the final state of analysis in the Basel group. So far total cross sections, invariant mass distributions, and beam-helicity asymmetries have been published in [23, 31] for free protons and incident photon energies up to 800 MeV. Quasi-free Data for $gamman \to p\pi^-\pi^0$ also up to energies of 800 MeV have been published in [40]. Beam-helicity asymmetries for quasi-free protons and neutrons up to 1.4 GeV have been published in [41]. Preliminary results for the total cross section of the free $\gamma p \to n\pi^0\pi^+$ reaction (S. Abt., priv. com) are shown in Fig. 5 together with their decomposition into different reaction types. This decomposition (neglecting interference patterns) has been obtained by a simultaneous fit of the $n\pi^0$, $n\pi^+$, and $\pi^0\pi^+$ invariant mass distributions with Monte Carlo simulations of the respective line shapes. Examples for these fits are shown in Appendix B 3.2. The following contributions were considered: $\gamma p \to n\pi^+\pi^0$ phase-space (blue symbols), the $\Delta^0(1232)\pi^+$ (red symbols) and $\Delta^+(1232)\pi^0$ (yellow symbols) intermediate states, and the $\gamma p \to n\rho^+$ reaction. A final analysis will of course require a more detailed model including also other reaction types (like $N^\star\pi$ intermediate states) and interference patterns, but the most important features can already be discussed with this simple analysis. The contributions of the $\Delta^0(1232)\pi^+$ and $\Delta^+(1232)\pi^0$ intermediate states are much different. This was expected because the $\Delta^+\pi^0$ intermediate state results mostly from sequential resonance decays of the $\gamma p \to N^\star, \Delta^\star \to \Delta(1232)^+\pi^0 \to n\pi^+\pi^0$ type while the $\Delta^0(1232)\pi^+$ intermediate state is also fed by $\Delta$-Kroll-Rudermann and pion pole terms which produce a $\Delta^0\pi^+$ pair at the first reaction vertex. Such diagrams are of course forbidden for neutral pions to which the incident photon cannot couple (and thus also not present in the $\gamma p \to p\pi^0\pi^0$ reaction). Very interesting is a comparison of the contributions from the $Delta^+\pi^0$ intermediate state and the $\rho$ production. Both contributions show a pronounced peak in the the energy range of the second nucleon resonance bump, actually it are these two reactions which are responsible for the peak-like structure in this energy range. In analogy to the behavior of $\pi^0$ pair production, the peak in the $Delta^+\pi^0$ intermediate state can be attributed to the sequential decay of the $D_{13}(1520)$ resonance via the $\Delta 1232)\pi$ intermediate state. The most probable source of $\rho$ meson emission is then the $D_{13}(1520)N\rho$ decay, since this resonance is the only state in the energy range of interest with a significant coupling to $N\rho$. The excitation curves do not exactly agree, however, one should keep in mind that no interference patterns are considered in this analysis. The strength of the two components in the $D_{13}$ range is very similar, so that the $N\rho$ decay of the $D_{13}$ seems to be comparable to its sequential decay over the $\Delta$. This is in agreement with the values listed in the Review of Particle Physics (PDG) which quotes branching ratios of 15 - 25% for both decay modes (the present data will probably allow a more precise determination of these values).

Similar data for photoproduction of quasi-free nucleons bound in the deuteron are also under analysis in the Basel group (S. Lutterer, priv. com.) so that also for this channel we will have a solid base for the elementary cross section off nucleons.

The perspectives for photoproduction of heavy nuclei are such as follows. When model results predicting strong in-medium modifications of the $\rho$ meson and related in-medium modifications of the $D_{13}$ resonance are correct, this must have significant and different implications for photoproduction of $\pi^0\pi^0$ and $\pi^\pm\pi^0$ pairs of nuclei. In case of the $\pi^0\pi^0$ final state mainly the overall change of the line-shape of the $D_{13}$ resonance due to the coupling to the modified $\rho$ would matter. However, for the $\pi^\pm\pi^0$ final state additionally a large effect from the modification of the partial width for the $N\rho$ decay would contribute (actually a smaller inverse effect should arise for $\pi^0$ pairs). Altogether, a clear modification of the partial widths for the decays into $\pi^0\pi^0$ and $\pi^\pm\pi^0$ pairs should arise. This can be investigated by a comparison of the cross sections from heavier nuclei normalized to the deuteron cross section for both reaction channels. This comparison will be even possible without the decomposition of the nuclear cross sections into their different components, although of course such a decomposition would strongly enhance the sensitivity for the effect (but may be difficult due to the stronger Fermi smearing and FSI for heavy nuclei).

## 1.3 Previous Results for Photoproduction of Pion-Pairs off Heavy Nuclei

Data for photoproduction of pion pairs off heavier nuclei are very sparse and have been measured in a different context. Three experiments at MAMI in Mainz [36–38] aimed at a possible in-medium modification of the $\sigma$ mesons and studied in detail the $\gamma A \to X\pi^0\pi^0$ reaction for several nuclei close to the production threshold, using photoproduction of $\pi^\pm\pi^0$ pairs (for which the scalar, isoscalar $\sigma$ cannot contribute) for comparison. Typical results for total cross sections are summarized in Fig. 6, left hand side. They do not allow a study of the line-shape of the second resonance region. The data from Messchendorp et al., and Bloch et al. [36,37] cover only energies up to 800 MeV and the data from Maghrbi et al. [38] even only up to 600 MeV. However, as an example, medium modifications of the

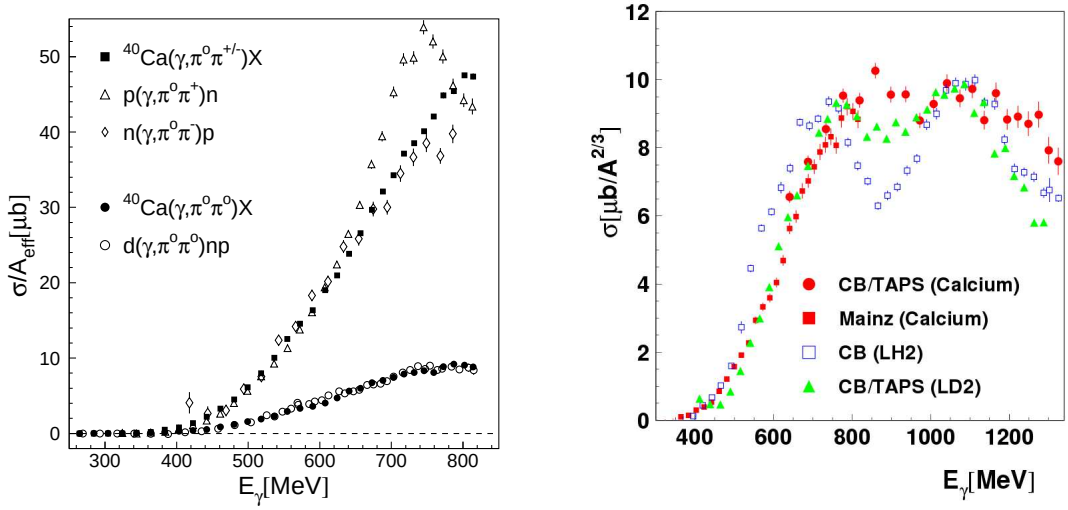


Figure 6: Left hand side: Total cross sections for $\pi^0\pi^0$ and $\pi^0\pi^\pm$ photoproduction off $^{40}$Ca [36] compared to $d(\gamma,\pi^0\pi^0)np$ [32] respectively to $p(\gamma,\pi^0\pi^+)n$ [23] and $n(\gamma,\pi^0\pi^-)p$ [40]. Cross sections are normalized to $A_{eff} = A^{2/3}$ for calcium and $A_{eff} = A$ for $A = 1, 2$. Right hand side: preliminary data from ELSA for the $\gamma^{40}Ca \to X\pi^0\pi^0$ reaction [39] compared to elementary cross sections.

$D_{13}(1520)$ line-shape as predicted by Post, Leupold, and Mosel [3] (see Fig 2) could not be detected by just measuring the low-energy tail of the resonance bump. In addition, the early experiments [36, 37] used as photon detector only the TAPS calorimeter, covering only about one quarter of the solid angle, so that the suppression of background from triple pion production was much more difficult. This was not a problem for the threshold regions at which these experiments aimed, but complicated largely the data analysis for energies above the $\eta$ production threshold (roughly 600 MeV for heavy nuclei) due to the abundant events from the $\eta \to 3\pi^0$ and $\eta \to \pi^0\pi^+\pi^-$ decays. The only attempt to measure $\gamma A \to X\pi^0\pi^0$ at higher incident photon energies was made for a $^{40}$Ca target at the CBELSA/TAPS setup in Bonn (see Fig. 6, right hand side) [39]. The data might indicate some line-shape effect at higher incident photon energies, however, they were not analyzed in any detail (just a by-product of a measurement of $\eta$-photoproduction off heavy nuclei) and have not been published. Data for the production of mixed-charge pion pairs from nuclei at energies above 800 MeV, to our knowledge, have never been reported.

# 2 Proposed Experiment

We propose to measure the photoproduction of $\pi^0\pi^0$ and $\pi^\pm\pi^0$ pairs in quasi-free kinematics from atomic nuclei ranging over mass numbers 4 (He), 7 (Li), 12 (C), 40 (Ca), to 208 (Pb). Most of the data for the $^4$He target can be taken parasitically with the already scheduled measurement of photoproduction of $\pi\eta$ pairs of $^4$He (this experiment will run at least partly only using the high energy sections of the tagger so that not all data can be used for the present proposal).

For the photon beam we will use a circularly polarized beam (longitudinally polarized electrons). This is mainly motivated by the fact that previous experiments for double pion production off deuterons have shown already significant FSI effects on the scale of total cross sections, but basically no effect on the beam-helicity asymmetries measurable in double-meson production with a circularly polarized beam. This is, however, only a side aspect aiming at a better understanding of the FSI effects.

The main prospect of the experiment is the comparison of the evolution of double pion production reactions from the deuteron over light nuclei like $^4$He, $^7$Li, to very heavy ones like $^{208}$Pb. Data for the free proton and for deuterium targets are available, partly already published, partly still under analysis. The selection of target nuclei covers different aspects of the problem. The available results from liquid hydrogen and liquid deuterium targets fix the elementary cross sections off the (quasi)-free nucleon. $^4$He nuclei have a large density, so that density dependent in-medium effects are already large, but still only relatively small FSI effects. The heavier nuclei then have the full-blown in-medium and FSI effects.

The predicted in-medium effects on the $\rho$ meson and the related effects on the $D_{13}(1520)$ resonance should result in (different) modifications of the cross sections for photoproduction of the $\pi^0\pi^0X$ and $\pi^0\pi^\pm X$ final states from heavy nuclei. The in-medium modification of the $\rho$ mesons may result in a modification of the the line-shape of the $D_{13}$ resonance, which would influence both reaction channels. In addition, an in-medium modification of the $\rho$ would also influence the partial decay width of the $D_{13}$ for this two final states (because the $\rho^\pm$ decays to $\pi\pm\pi^0$, but the $\rho^0$ cannot decay to $\pi^0\pi^0$). Therefore, a comparison of the evolution with target mass for the two different decay channels should reveal

in-medium effects on the partial widths.

The identification of the reactions has already been studied with several previous experiments for proton and deuteron, but also for heavier target nuclei [34–36, 38, 41]. As an example we show in Fig. 7 the identification of charged pions by the $E - \Delta E$ method using CB and PID and the identification of $\pi^0$ pairs in a two-dimensional invariant mass spectrum for a $^7$Li target [38]. The figure refers to low incident photon energies, where the cross section in particular for $\pi^0\pi^0$ is verv small.

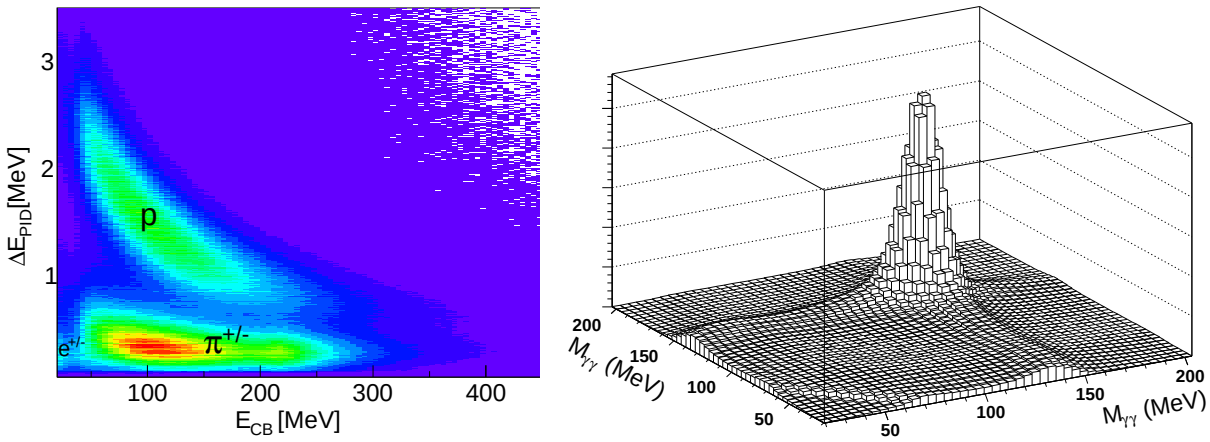


Figure 7: Reaction identification for a $^7$Li target [38]. Left hand side: Energy deposition in CB versus PID. Charged pions are separated from protons and low energy electrons. Right hand side: Two-dimensional distribution of the invariant masses from the $\pi^0\pi^0$ channel for incident photon energies between 400 - 460 MeV.

Background will mainly result from reactions with a three-pion final state (in particular $3\pi^0$ and $\pi^0\pi^+\pi^-$ from decays of the $\eta$ meson). The $\pi^0\pi^+\pi^-$ final state produces background when one of the two charged pions escapes detection (is stopped in the target or other inactive material) or is misidentified as a proton. The triple $\pi^0$ is only problematic, when either two decay photons escape detection or one escapes detection and the other is misidentified as a neutron. At higher incident photon energies some additional background will arise from $\eta\pi$ final states. Altogether, identification of the $\pi^0\pi^0$ final state is simpler (due to the double invariant mass filter) as for the $\pi^\pm\pi^0$ final state. Reaction identification will be mainly done with coplanarity and - even more important - missing mass analyses. As an example we show in Fig. 8 measured missing mass spectra for the $\gamma p \to n\pi^0\pi^\pm$ reaction and in Fig. 9 coplanarity spectra for the same reaction (S. Abt, priv. com.). Both types of spectra are for incident photon beam energy of 1.3 GeV (i.e. in a region with substantial background from competing reactions) and for different bins of the cosine of the cm polar angle of the pion-pion system. For the missing mass analysis the recoil nucleon (even when detected) is treated as missing particle and its mass is computed from the four vectors of the pions. The missing mass is then defined as:

$$\Delta m = |P_\gamma + P_N - P_{\pi^0} - P_{\pi^+}| - m_N \tag{2}$$

with the four vectors of the incident photon ($P_\gamma$, the target nucleon at rest ($P_N$), the four vectors of the pions ($P_{\pi^0}$, $P_{\pi^+}$, and the mass of the nucleon $m_N$.

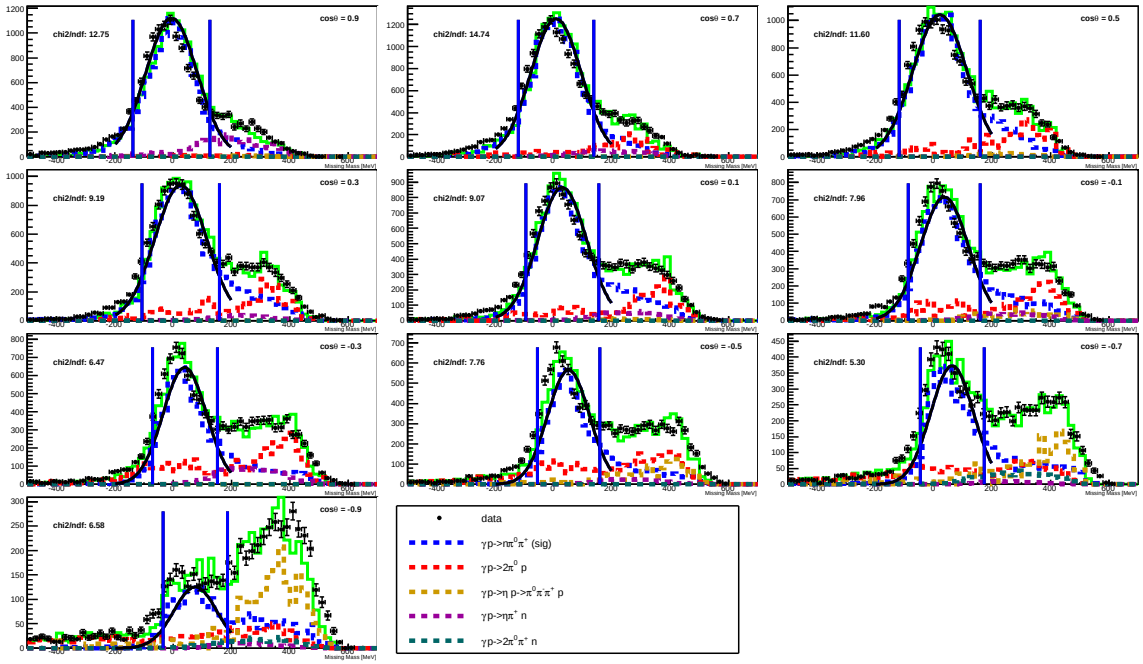


Figure 8: Missing mass spectra for identification of the reaction $\gamma p \to n\pi^0\pi^\pm$ for an incident photon energy of 1.3 GeV for different bins of $\cos(\Theta_{\pi\pi})$. Data (black dots) compared to MC simulations of the signal and several background reactions. Fractions of the background reactions fitted to data. Sum of all components (green histograms) are in good agreement with measured data (S. Abt, priv. com.).

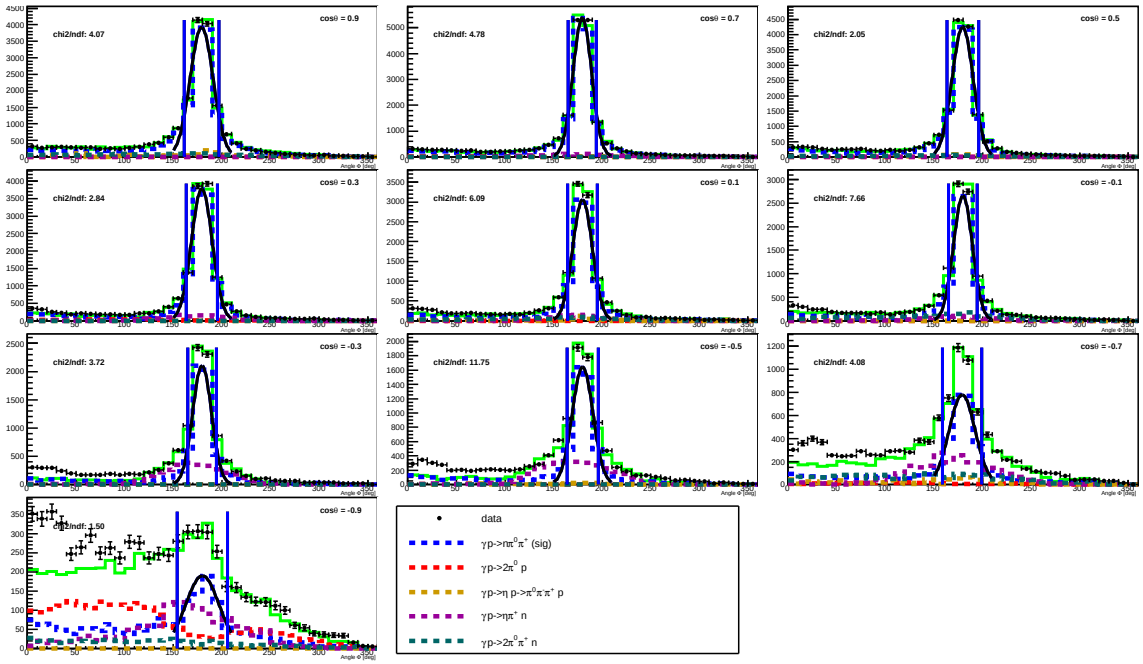


Figure 9: Coplanarity spectra for identification of the reaction $\gamma p \to n\pi^0\pi^\pm$ for an incident photon energy of 1.3 GeV for different bins of $\cos(\Theta_{\pi\pi})$. Notation as in Fig. 8

The coplanarity angle $\Delta\phi$ is defined by

$$\Delta\phi = \quad \phi_{\pi\pi} - \phi_N \quad \text{for} \quad \phi_{\pi\pi} - \phi_N \geq 0 \tag{3}$$

$$\Delta\phi = \quad 2\pi - |\phi_{\pi\pi} - \phi_N| \quad \text{for} \quad \phi_{\pi\pi} - \phi_N < 0 \tag{4}$$

For the free proton background in the region of the signal peak is only small, so that already a cut on the signal peak in the missing mass spectra would yield relatively clean reaction identification. For nuclear targets the signals will of course be smeared out by Fermi motion and FSI effects, which will complicate the analysis. However, it was already demonstrated in [36] that the $\pi^0\pi^0$ and $\pi^0\pi^\pm$ final states can be identified quite cleanly for a $^{40}$Ca target, even though in that experiment background from triple pion production (compare e.g. Fig. 4 in this reference) was much more abundant (because due to the small solid angle coverage many triple pion events appeared as pion pairs in the data stream) than it will be in the proposed experiment.

As a side remark one should mention that we would use these data of course also for further investigations for example for the study of $\eta\pi$ production off the heavier nuclei.

## 2.1 Count rate estimates

The usable target thickness is limited by the radiation length of the targets, so that loss rates due to conversion of photons to electron - positron pairs do not become unreasonable. We will use the same targets as have been used for the measurement of the low - energy production of pion pairs in [38]. Their properties are summarized in Tab. 1 and compared to the parameters of the liquid hydrogen target used for the results shown in Figs. 5,16,17,18.

Table 1: Main parameters of the targets. 1st column: Target type (remark: for Pb we will use a natural lead target isotopic pure 208 target is not necessary). 2nd column: target length [cm], 3rd column: target density density $\rho_s$ [g/cm$^3$], 4th column: target surface density [nuclei/barn], 5th column: mass number scaling of cross section $A^{2/3}$, 6th column: effective target nucleon surface density [effective number of nucleons/barn].

| Target | L[cm] | $\rho$[g/cm$^3$] | $\rho_s$[N/barn] | $A^{2/3}$ | $\rho_n[n_{\text{eff}}/\text{barn}]$ |
|---|---|---|---|---|---|
| $LH_2$ | 10.0 | 0.07 | 0.422 | 1.0 | 0.42 |
| L$^4$He | 5.0 | 0.123 | 0.093 | 2.5 | 0.23 |
| $^7$Li | 5.4 | 0.534 | 0.264 | 3.7 | 1.00 |
| $^{12}$C | 1.5 | 1.7 | 0.13 | 5.2 | 0.68 |
| $^{40}$Ca | 1.0 | 1.54 | 0.024 | 11.7 | 0.28 |
| $^{208}$Pb | 0.05 | 11.34 | 0.0019 | 139.0 | 0.26 |

The table gives the target lengths and the density of the target materials. This has been converted into the surface density of nuclei in the targets $\rho_s$. The relevant parameter for the estimate of count rates is this density times the nuclear cross sections. Since, due to the strong absorption of pions in nuclear matter, the quasi-free production cross sections off nuclei scale with $A^{2/3}$, where $A$ is the nuclear mass number the product $\rho_s \times A^{2/3}$ goes linearly into the observed count rates. This parameter is given in the last column of the

table. With this target parameters we can achieve higher production rates than with the liquid hydrogen target for Li and C and about 2/3 of the rates for Ca and Pb. The lowest rates are expected for the $^4$He target, however, since those data can be taken together with the longer beam time for the measurement of coherent $\eta\pi$ production in view of $\eta$ mesic nuclei this does not matter.

With the above numbers we can also give a rough estimate of achievable count rates in absolute numbers. The elementary cross sections for the production of pairs off the nucleon are around 10 $\mu b$ ($\pi^0\pi^0$) and between 15-40 $\mu b$ ($\pi^0\pi^\pm$), respectively. We will tag the energy range from 400 - 1600 MeV and use a 4 mm collimator. This means the average photon flux (if the experiment is done with the old tagger) will be $\approx 0.6\times10^6$ electrons per second for a 4 MeV wide bin multiplied with a tagging efficiency of $\approx$0.66%. This translates for the production of $\pi^0\pi^0$ pairs of the lead target to a reaction rate of $N_{\pi^0\pi^0}$:

$$N_{\pi^0\pi^0} = 0.26/b\times4\times10^5/(s\times4MeV)\times12\mu b\times\epsilon_{det}\times t_{lf} = 1.25/(s\times4MeV)\times\epsilon_{det}\times t_{lf}, \quad (5)$$

where $\epsilon_{det}$ is the detection efficiency and $t_{lf}$ is the experiment life time, for which we assume $\approx$70%. The detection efficiency is much dependent on the event conditions. The lowest values are obtained when the full final state for recoil neutrons is requested (i.e. final states with $\pi^0\pi^0 n$ or $\pi^0\pi^+ n$). In this case values around 5% are realistic for $\epsilon_{det}$. Since about half of the events will be due to final state recoil nucleons we can expect a detected average rate of 0.02/(s$\times$ 4MeV) for $\pi^0$ pairs in coincidence with neutrons, while for protons in coincidence with $\pi^0\pi^-$ pairs (detection efficiency around 20%) average detected reaction rates of 0.28/(s$\times$ 4MeV) might be reached. Thus for the lead target we can expect about 7000 events in 100 h for the most critical reaction and around 100000 events for the least critical reaction (which will allow to use quite stringent cuts for background suppression). Altogether on average 100 h of beam time per target (for the Li, C, Ca, Pb) targets will be sufficient to measure statistically well defined results.

# 3 Appendices

## 3.1 Appendix A: Experimental Setup

### 3.1.1 Photon Beam

The A2 photon beam is derived from the production of Bremsstrahlung photons during the passage of the MAMI electron beam through a thin radiator. The resulting photons can be circularly polarized, with the application of a polarized electron beam, or linearly polarized, in the case of a crystalline radiator. The degree of polarization achieved is dependent on the energy of the incident photon beam ($E_0$) and the energy range of interest, but currently peaks at ∼75 % for linear polarization and ∼85 % for circular polarization (Fig. 10). The experiment proposed here will only use circularly polarized photon beams.

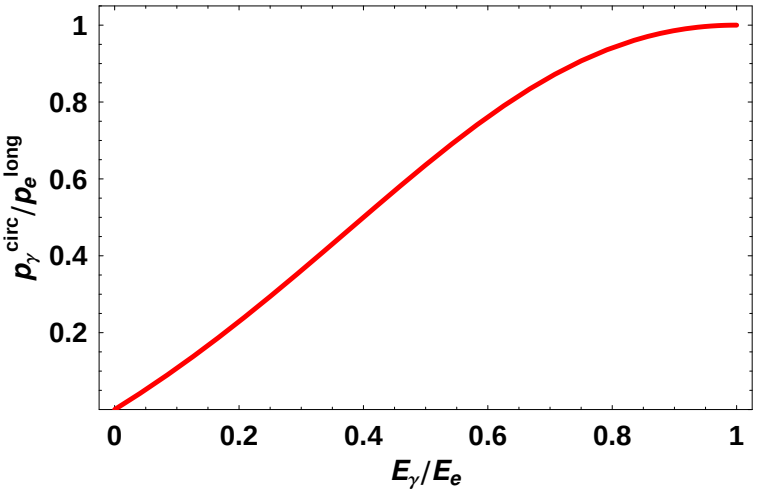


Figure 10: Helicity transfer from the electron to the photon beam as function of the energy transfer. The MAMI beam polarization is $P_e$ =85%.

The Glasgow-Mainz Photon Tagger (Fig 11) provides energy tagging of the photons by detecting the post-radiating electrons and can determine the photon energy with a resolution of 2 to 4 MeV depending on the incident beam energy, with a single-counter time resolution $\sigma_t$ = 0.17 ns [44]. Each counter can operate reliably to a rate of ∼ 1 MHz, giving a photon flux of $2.5 \times 10^5$ photons per MeV. Photons can be tagged in the momentum range from 4.7 to 93.0% of $E_0$.

To augment the standard focal plane detector system and make use of the Tagger's intrinsic energy resolution of 0.4 MeV (FWHM), there exists a scintillating fiber detector ("Tagger Microscope") that can improve the energy resolution by a factor of ∼6 for a ∼100MeV wide region of the focal plane (dependent on its position) [47].

### 3.1.2 Targets

The proposed experiment does not need the A2 polarized buthanol target but a liquid $^4$He target and solid state targets (Li, C, Ca, Pb). A liquid He target had been constructed in collaboration of the Mainz and Basel groups some years ago for the measurement of $\eta$ photoproduction off $^3$He for the search for $\eta$-mesic nuclei [45] (see Fig. 12). This target

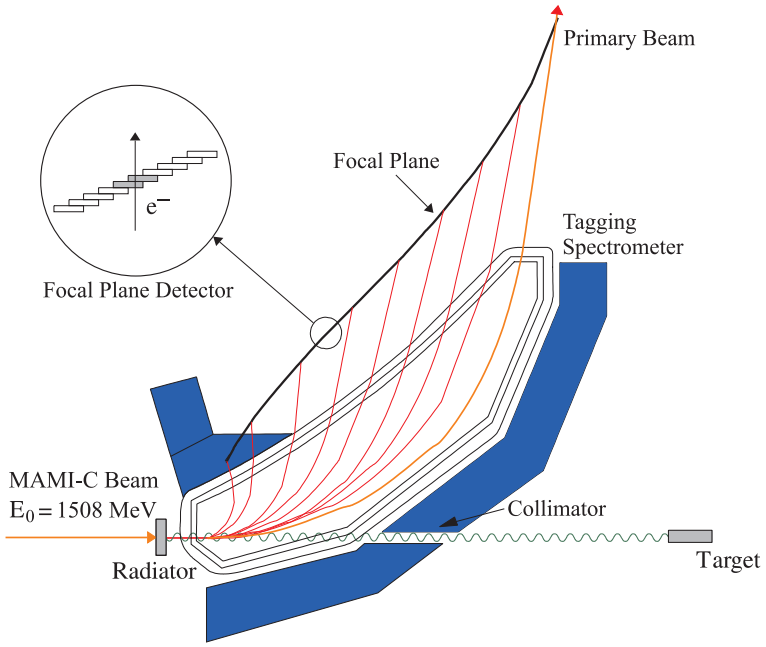


Figure 11: The Glasgow-Edinburgh-Mainz photon tagging spectrometer

is currently being maintenanced and slightly modified for the (less critical use) with $^4$He and will be used in the near future for the measurement of photoproduction of $\eta\pi$ pairs also in view of $\eta$-mesic nuclei. Most of the beam time for the $^4$He measurement proposed here can be taken together with this experiment.

The other targets are simple solid state targets (blocks of Li, C, slices of Ca and Pb) which only have to be mounted in an evacuated beam tube and do not require any particular preparations (target materials are available, have already been used for previous experiments).

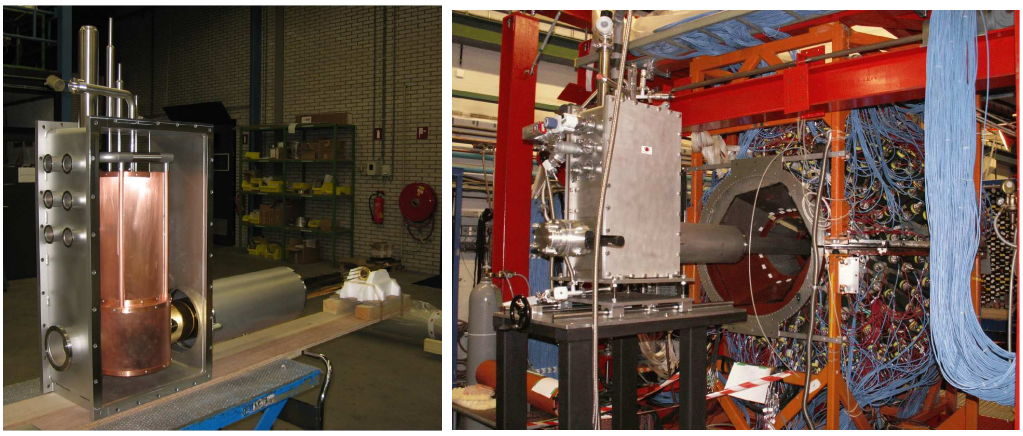

Figure 12: Liquid He cryo target of the A2-collaboration

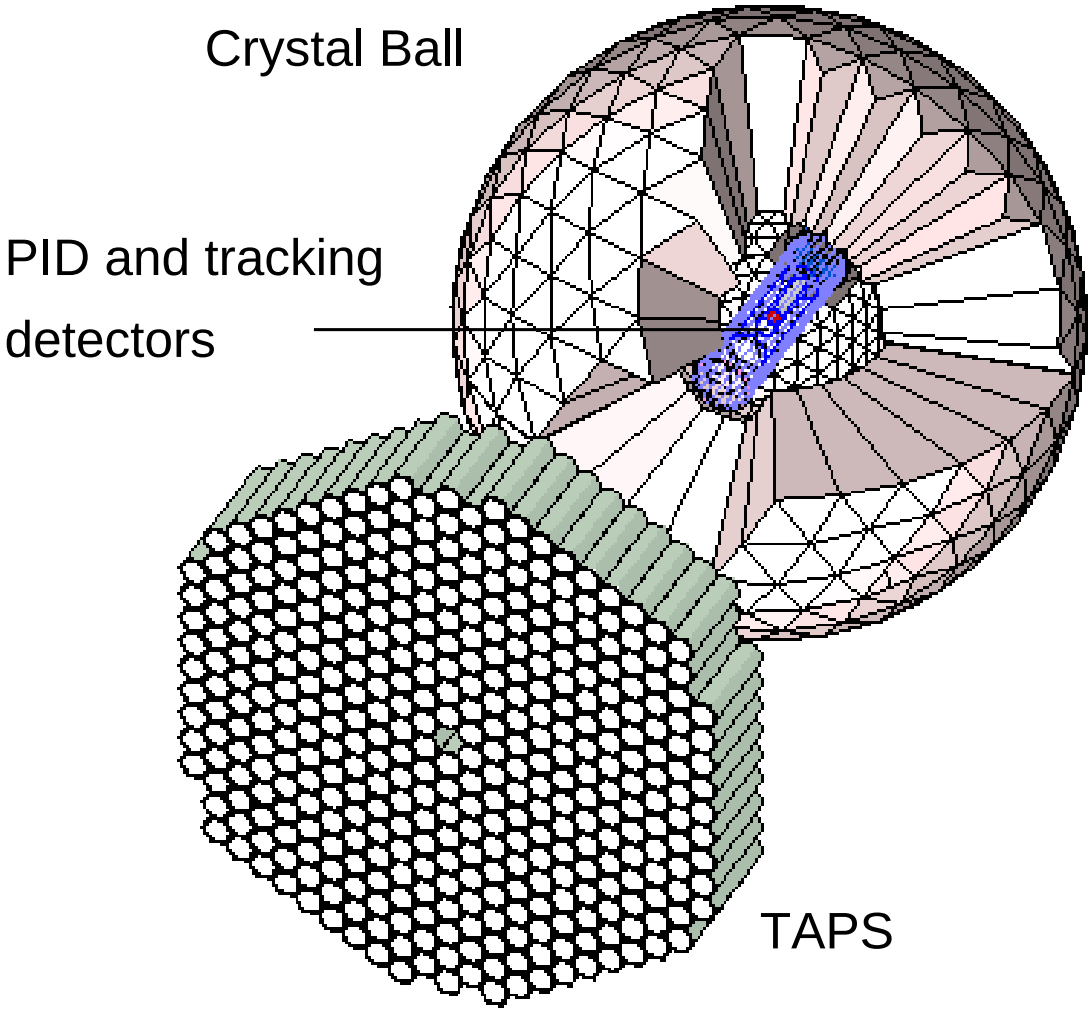


Figure 13: The A2 detector setup: the Crystal Ball calorimeter with cut-away section showing the inner detectors and the TAPS forward wall.

### 3.1.3 Crystal Ball Detector System

The central detector system consists of the Crystal Ball calorimeter combined with a barrel of scintillation counters for particle identification and two coaxial multiwire proportional counters for charged particle tracking. This central system provides position, energy and timing information for both charged and neutral particles in the region between 21° and 159° in the polar angle, $\theta$, and over almost the full azimuthal ($\phi$) range. At forward angles, less than 21°, reaction products are detected in the TAPS forward wall. The full, almost hermetic, detector system is shown schematically in Fig. 13 and the measured two-photon invariant mass spectrum is shown in Fig. 14.

The Crystal Ball detector is a highly segmented 672-element NaI(Tl), self triggering photon spectrometer constructed at SLAC in the 1970's. Each element is a truncated triangular pyramid 41 cm (l5.7 radiation lengths) long. The Ball has an energy resolution of $\Delta E/E = 0.020(E[GeV])^{0.36}$, an angular resolution in $\sigma_\theta$ of $2-3°$ and $\sigma_\phi$ of $\sigma_\theta/\sin\theta$ for electromagnetic showers [43]. The readout electronics for the Crystal Ball were completely renewed in 2003, and it now is fully equipped with SADCs which allow for the full sampling of pulse-shape element by element. In normal operation, the onboard summing capacity of

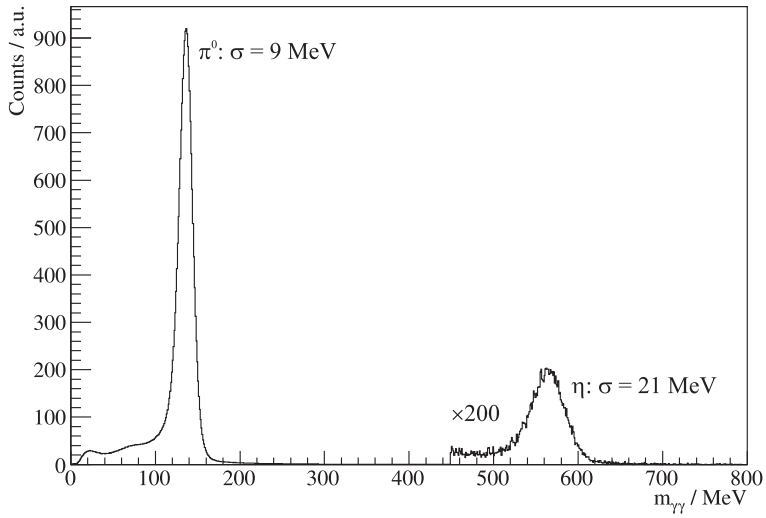


Figure 14: Two gamma invariant mass spectrum for the CB TAPS detector setup. Both $\eta$ and $\pi^0$ mesons can be clearly seen.

these ADCs is used to enable dynamic pedestal subtraction and the provision of pedestal, signal and tail values for each element event-by-event. Each CB element is also newly equipped with multi-hit CATCH TDCs. The readout of the CB is effected in such a way as to allow for flexible triggering algorithms. There is an analogue sum of all ADCs, allowing for a total energy trigger, and also an OR of groups of sixteen crystals to allow for a hit-multiplicity second-level trigger - ideal for use when searching for high multiplicity final states.

In order to distinguish between neutral and charged particles species detected by the Crystal Ball, the system is equipped with PID 2, a barrel detector of twenty-four 50 mm long 4 mm thick scintillators, arranged so that each PID 2 scintillator subtends an angle of 15° in $\phi$. By matching a hit in the PID 2 with a corresponding hit in the CB, it is possible to use the locus of the $\Delta$E, E combination to identify the particle species (Fig. 15). This is primarily used for the separation of charged pions, electrons and protons. The PID 2 covers from 15° to 159° in $\theta$.

The excellent CB position resolution for photons stems from the fact that a given photon triggers several crystals and the energy-weighted mean of their positions locates the photon position to better than the crystal pitch. For charged particles which deposit their energy over only one or two crystals, this is not so precise. Here the tracks of charged particles emitted within the angular and momentum acceptance of the CB detector will be reconstructed from the coordinates of point of intersections of the tracks with two coaxial cylindrical multiwire proportional chambers (MWPCs) with cathode strip readout. These MWPCs are similar to those installed inside the CB during the first round of MAMI-B runs [46]. The most significant difference is that all detector signals are taken at the upstream end of the MWPCs, minimizing the material required and facilitating particle detection in the forward polar region.

A mixture of argon (79.5%), ethane (30%) and freon-$CF_4$ (0.5%) is used as the filling gas. This mixture is a compromise between charge multiplication and localization requirements imposed by the ionizing particle tracks.

Within each chamber both the azimuthal and the longitudinal coordinates of the

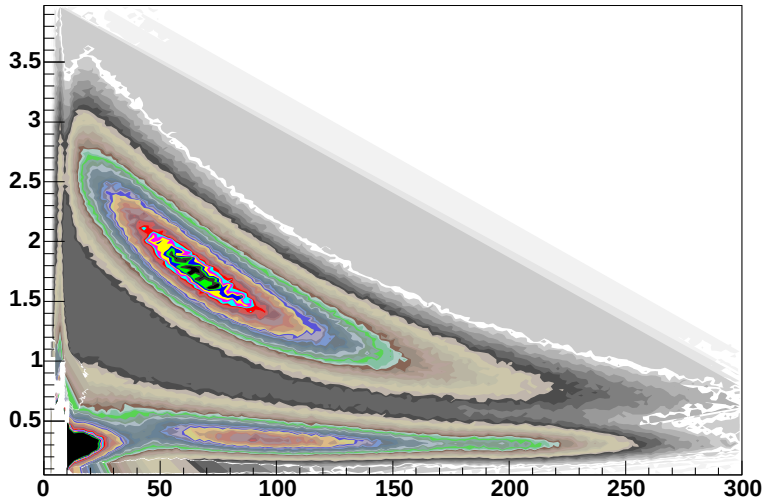


Figure 15: A typical ΔE/E plot from the PID detector. The upper curved region is the proton locus, the lower region contains the pions and the peak towards the origin contains mostly electrons.

avalanche will be evaluated form the centroid of the charge distribution induced on the cathode strips. The location of the hit wires(s) will be used to resolve ambiguities which arise from the fact that each pair of inner and outer strip cross each other twice. The expected angular resolution (rms) will be $\approx 2^\circ$ in the polar emission angle $\vartheta$ and $\approx 3^\circ$ in the azimuthal emission angle $\varphi$.

The MWPCs have been recently installed inside the CB frame and their calibration using both cosmic rays and test beam data is currently underway.

### 3.1.4 TAPS Forward Wall

The TAPS forward wall is composed of 384 $BaF_2$ elements, each 25cm in length (12 radiation lengths) and hexagonal in cross section, with a diameter of 59 mm. Every TAPS element is covered by a 5 mm thick plastic veto scintillator. The single counter time resolution is $\sigma_t = 0.2$ ns. The energy resolution can be described by the $\Delta E/E = 0.018 + 0.008/(E[GeV])^{0.5}$ [43]. The angular resolution in the polar angle is better than 1°, and in the azimuthal angle it improves with increasing $\theta$, being always better than 1/R radian, where R is the distance in centimeters from the central point of the TAPS wall surface to the point on the surface where the particle trajectory meets the detector. The TAPS readout was custom built for the beginning of the CB@MAMI program and is effected in such a way as to allow particle identification by Pulse-Shape Analysis (PSA), Time-of-Fight (TOF) and ΔE/E methods (using the energy deposit in the plastic scintillator to give ΔE). TAPS can also contribute to the CB multiplicity trigger and is currently divided into up to six sectors for this purpose.

## 3.2 Appendix B: invariant mass distributions for pion-pion and pion-nucleon pairs for the $\gamma p \to n\pi^0\pi^+$ reaction

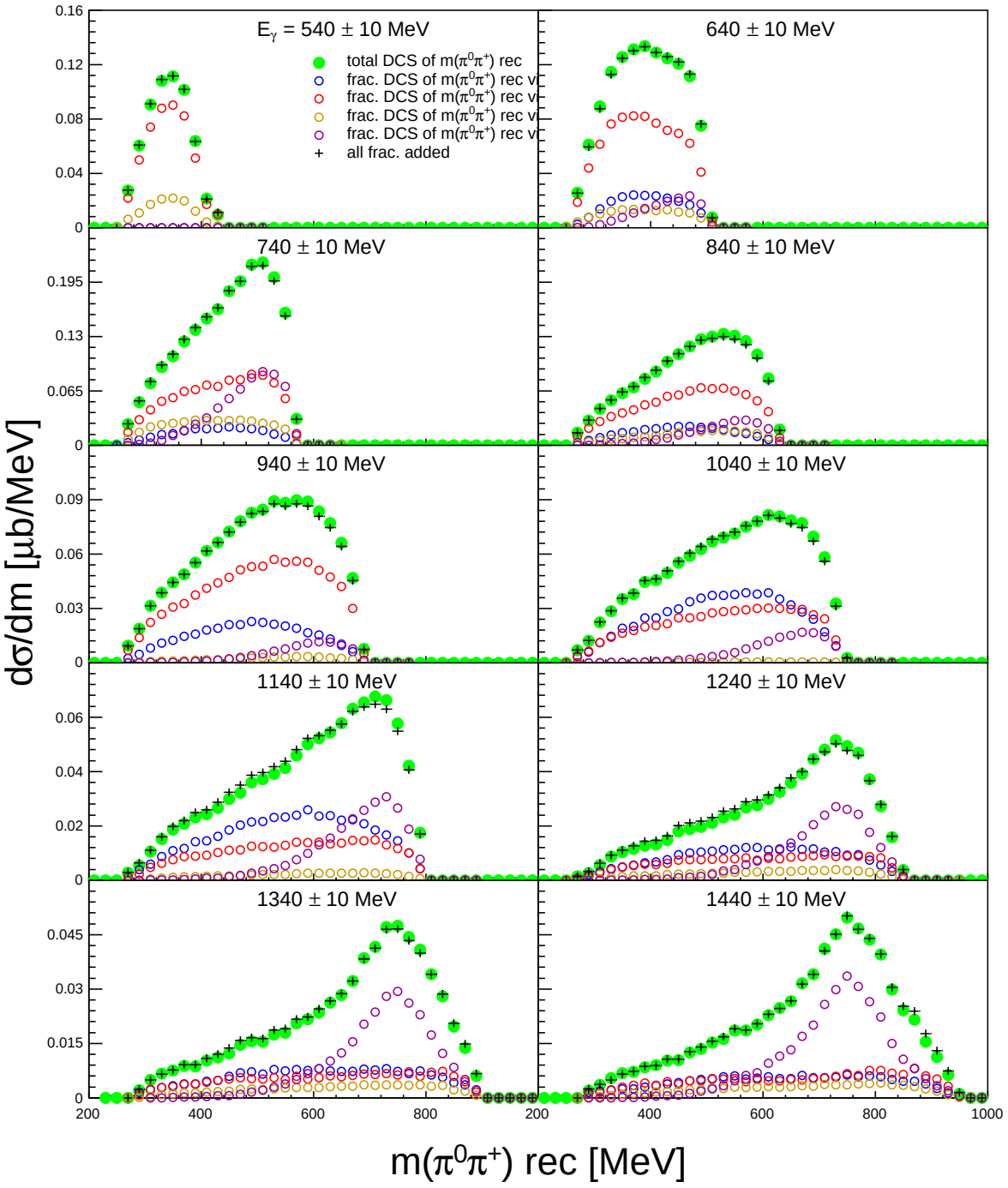


Figure 16: Invariant mass distributions of the $\pi^0\pi^+$ pairs from the $\gamma p \to n\pi^0\pi^+$ reaction. Note the large contribution from the $\gamma p \to n\rho^+$ intermediate state (purple symbols) around incident photon energies of the second resonance bump (≈740 MeV) and at high incident photon energies (color code as in Fig. 5, S. Abt, preliminary results).

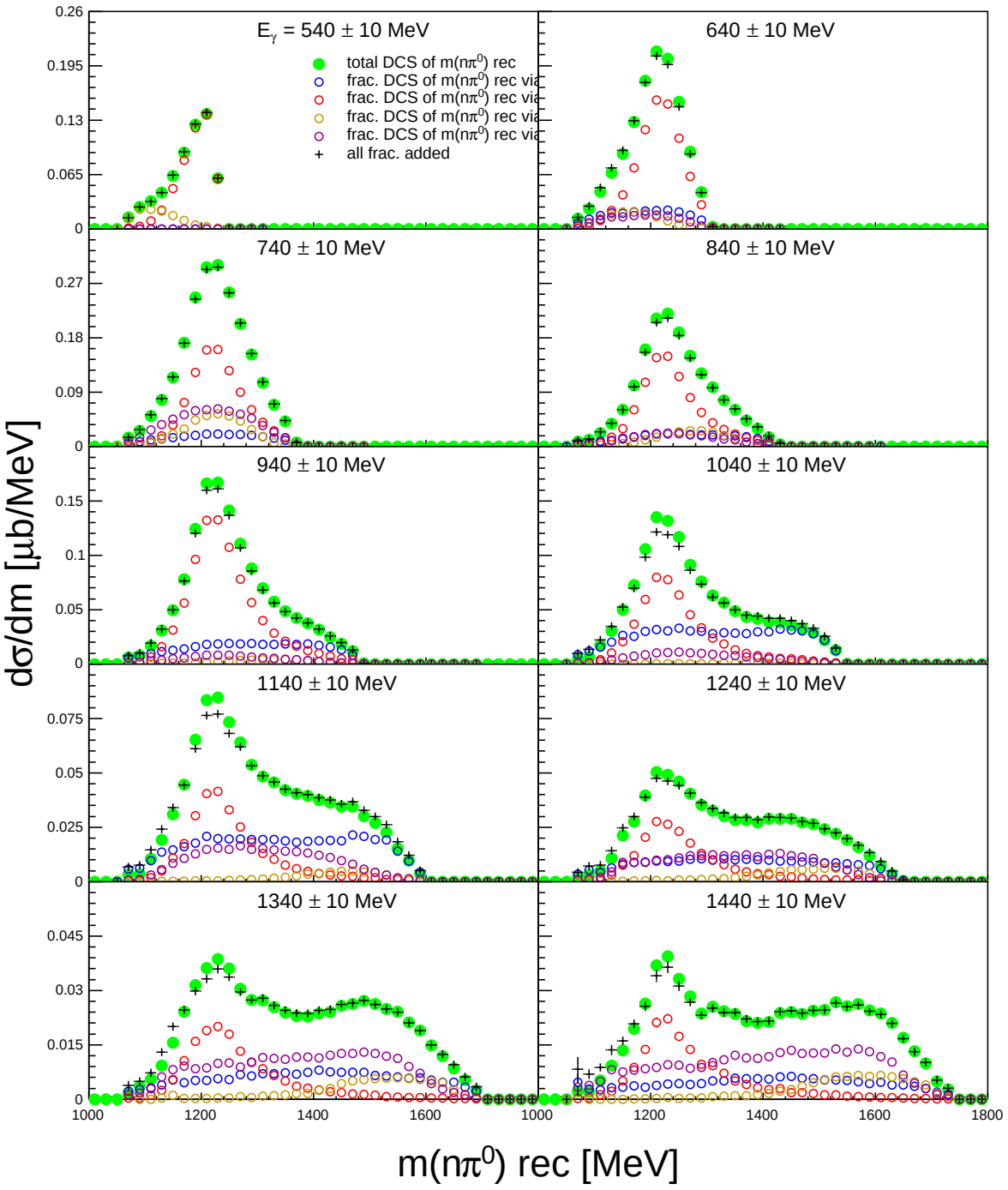


Figure 17: Invariant mass distributions of the $\pi^0 n$ pairs from the $\gamma p \to n\pi^0\pi^+$ reaction. The pronounced peak around 1232 MeV is due to the $\Delta\pi^0$ intermediate state which is fed by sequential decay chains of the type $\gamma p \to N^\star, \Delta^\star \to \Delta(1232)\pi^+ \to n\pi^0\pi^+$ but also by $\Delta$-Kroll-Rudermann diagrams for which at the photon reaction vertex a charged-pion-$\Delta^0$ pair is produced. (color code as in Fig. 5, S. Abt, preliminary results).

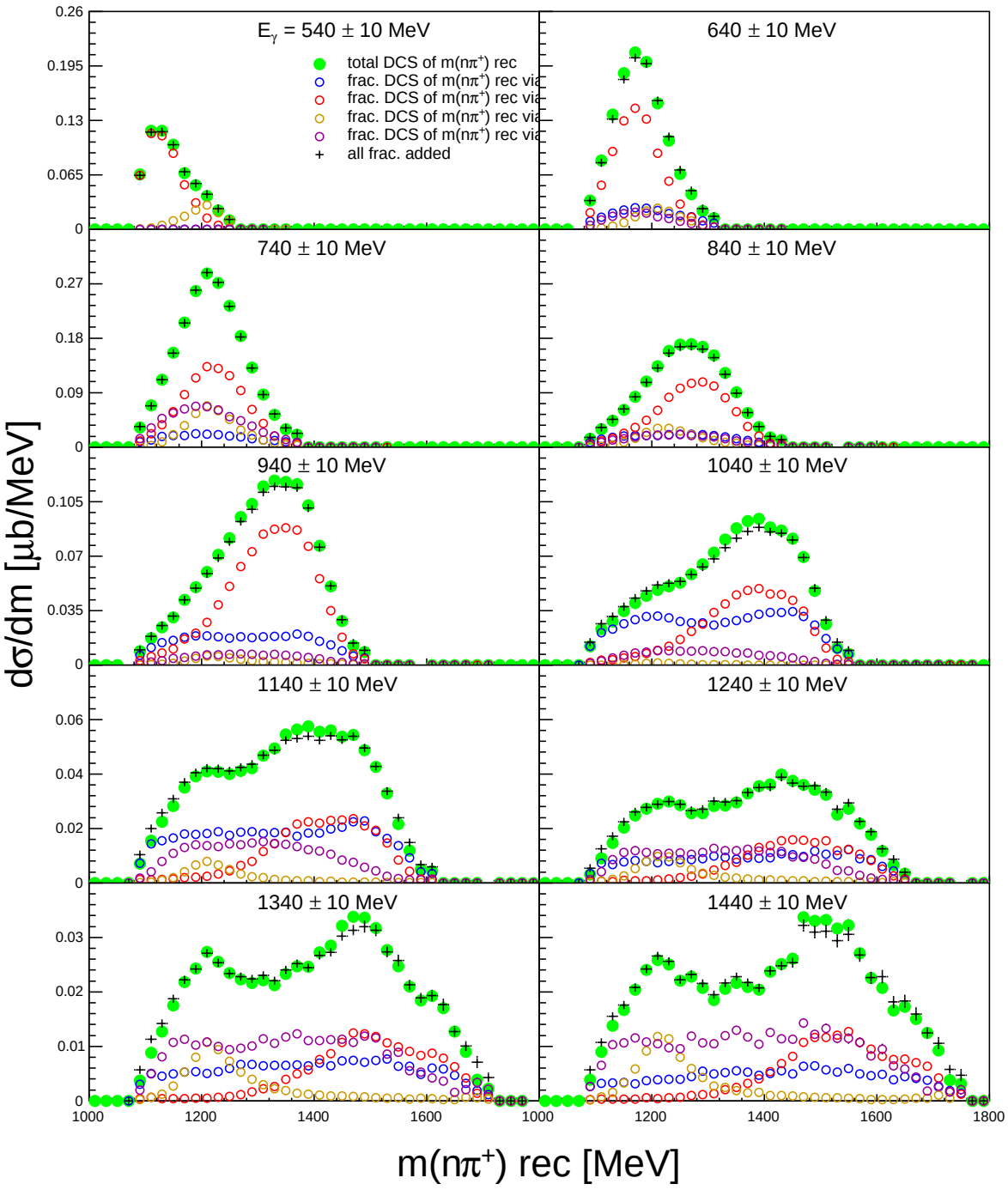


Figure 18: Invariant mass distributions of the $\pi^+ n$ pairs from the $\gamma p \to n\pi^0\pi^+$ reaction. In this case the peak around 1232 MeV is much less pronounced because the $\Delta$-Kroll-Rudermann diagrams for neutral-pion-$\Delta^+$ pairs are strongly suppressed (most of the strength comes from the sequential resonance decays). (color code as in Fig. 5,S. Abt, preliminary results).

# References


[1] M. Lutz *et al.*, Nucl. Phys., **A 542**, 521 (1992).

[2] G.E. Brown and M. Rho, Phys. Rev. Lett. **66**, 2720 (1991).

[3] M. Post et al., Nucl. Phys. **A 741**, 81 (2004).

[4] S. Leupold, V. Metag, U. Mosel, Int. J. of Mod. Phys. **E 19**, 147 (2010).

[5] R. Nasseripour et al., Phys. Rev. Lett. **99**, 262302 (2007).

[6] M.H. Wood *et al.*, Phys. Rev. **C 78**, 015201 (2008).

[7] N. Bianchi *et al.*, Phys. Lett. **B 325**, 333 (1994).

[8] B. Krusche *et al.*, Eur. Phys. J. **A 6**, 309 (1999).

[9] K. Büchler *et al.*, Nucl. Phys. **A 570**, 580 (1994).

[10] A. Braghieri *et al.*, Phys. Lett. **B 363**, 46 (1995).

[11] B. Krusche *et al.*, Phys. Rev. Lett. **74**, 3736 (1995).

[12] M. MacCormick *et al.*, Phys. Rev. **C 53**, 41 (1996).

[13] F. Härter *et al.*, Phys. Lett. **B 401**, 229 (1997).

[14] M. Wolf *et al.*, Eur. Phys. J. **A 9**, 5 (2000).

[15] Th. Frommhold et al., Phys. Lett. **B 295**, 28 (1992).

[16] N. Bianchi *et al.*, Phys. Lett. **B 299**, 219 (1993).

[17] B. Krusche, Prog. Part. Nucl. Phys. **55**, 46 (2005).

[18] L.A. Kondratyuk *et al.*, Nucl. Phys. **A 579**, 453 (1994).

[19] W.M. Alberico *et al.*, Phys. Lett. **B 321**, 177 (1994).

[20] J. Lehr *et al.*, Nucl. Phys. **A 671**, 503 (2000).

[21] B. Krusche and S. Schadmand, Prog. Part. Nucl. Phys. **51**, 399 (2003).

[22] A. Zabrodin *et al.*, Phys. Rev. **C 60**, 055201 (1999).

[23] W. Langgärtner *et al.*, Phys. Rev. Lett. **87**, 052001 (2001).

[24] U. Thoma *et al.*, Phys. Lett. **B 659**, 87 (2008).

[25] A.V. Sarantsev *et al.*, Phys. Lett. **B 659**, 94 (2008).

[26] V. Kashevarov *et al.*, Phys. Rev. **C 85**, 064610 (2012).

[27] F. Zehr *et al* Eur. Phys. J. **A 48**, 98 (2012).

[28] A. Thiel *et al.*, Phys. Rev. Lett. **114**, 091803 (2015).

[29] V. Sokhoyan *et al.*, Phys. Lett. **B 746**, 127 (2015).

[30] V. Sokhoyan *et al.*, Eur. Phys. J. **A 51**, 95 (2015).

[31] D. Krambrich *et al.*, Phys. Rev. Lett. **103**, 052002 (2009).

[32] V. Kleber *et al.*, Eur. Phys. J. **A 9**, 1 (2000).

[33] J. Ajaka *et al.*, Phys. Lett. **B 651**, 108 (2007).

[34] M. Oberle *et al.*, Phys. Lett. **B 721**, 237 (2013).

[35] M. Dieterle *et al.*, Eur. Phys. J. **A 51**, 142 (2015).

[36] F. Bloch *et al.*, Eur. Phys. J. **A 32**, 219 (2007).

[37] J.G. Messchendorp *et al.*, Phys. Rev. Lett. **89**, 222302 (2002).

[38] Y. Maghrebi *et al.*, Phys. Lett. **B 722**, 69 (2013).

[39] Th. Mertens, PhD thesis, University of Basel, 2006

[40] A. Zabrodin *et al.*, Phys. Rev. **C 55**, R1617 (1997), and P. Pedroni priv. com.

[41] M. Oberle *et al.*, Eur. Phys. J. **A 50**, 54 (2014).

[42] K.A. Olive *et al.*, Cin. Phys. **C 38**, 090001 (2014).

[43] S. Prakhov *et al.*, Phys. Rev. **C 79**, 035204 (2009).

[44] J. C. McGeorge *et al.*, Eur. Phys. J. **A 37**, 129 (2008).

[45] F. Pheron *et al.*, Phys. Lett. **B 709**, 21 (2012).

[46] G. Audit *et al.*, Nucl. Instr. Meth. **A 301**, 473 (1991).

[47] A. Reiter *et al.*, Eur. Phys. J. **A 30**, 461 (2006).